Computational Methods for Ideal Magnetohydrodynamics

Andrew Kercher

A defense of the dissertation submitted in partial fulfillment of the requirements for the degree of Doctor of Philosophy
George Mason University

25 August 2014

Introduction

- Compound wave formation in MHD bow shock simulations.

Introduction

- Compound wave formation in MHD bow shock simulations.
- Compound wave product of numerical diffusion.

Introduction

- Compound wave formation in MHD bow shock simulations.
- Compound wave product of numerical diffusion.
- Slow convergence with finite volume schemes.

Introduction

- Compound wave formation in MHD bow shock simulations.
- Compound wave product of numerical diffusion.
- Slow convergence with finite volume schemes.
- Compound wave modification (CWM).
  - Modification to the HLLD approximate Riemann solver.
  - Removes compound wave, correctly computes rotational discontinuity.
  - Converges at all grid resolutions.
  - FAST! HLLD intermediate states are already calculated.

Introduction

- Compound wave formation in MHD bow shock simulations.
- Compound wave product of numerical diffusion.
- Slow convergence with finite volume schemes.
- Compound wave modification (CWM).
  - Modification to the HLLD approximate Riemann solver.
  - Removes compound wave, correctly computes rotational discontinuity.
  - Converges at all grid resolutions.
  - FAST! HLLD intermediate states are already calculated.
- Description multi-dimensional fluid solver capable of shared memory parallelism.
  - Hydrodynamics and ideal MHD.
  - Algorithms implemented for unstructured grids.

Space Weather

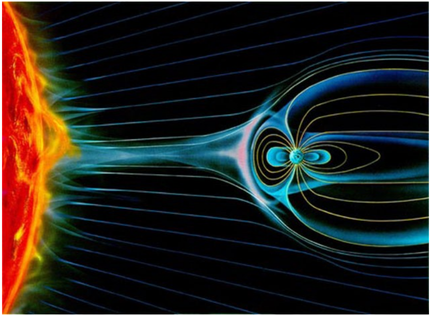

- Sun-earth interaction:

Space Weather

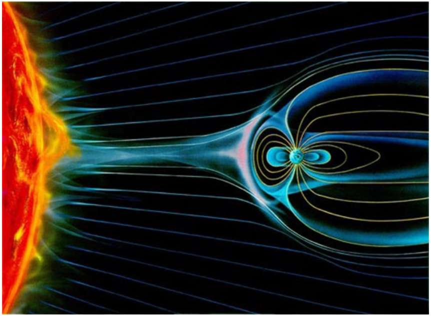

- 2D ideal MHD bow shock simulation. [1]
  - Results contained intermediate shocks.

Space Weather

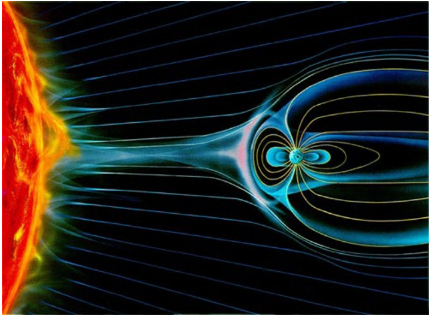

- 2D ideal MHD bow shock simulation. [1]
  - Results contained intermediate shocks.
  - Intermediate shocks considered inadmissible in ideal MHD [5]

Space Weather

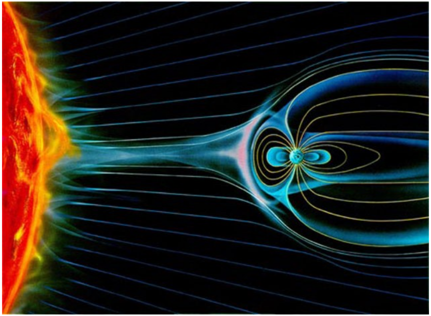

- 2D ideal MHD bow shock simulation. [1]
  - Results contained intermediate shocks.
  - Intermediate shocks considered inadmissible in ideal MHD [5]
  - Cause?

Riemann Problems

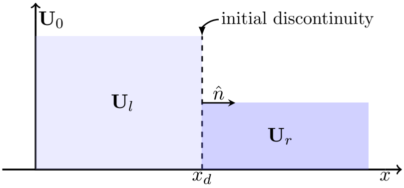

- Initial discontinuity at x_d separates two constant states.

$$\frac{\partial \mathbf{U}}{\partial t} + \frac{\partial \mathbf{F}}{\partial \mathbf{x}} = \mathbf{0} \ ,$$

$$\mathbf{U}_0 = \begin{cases} \mathbf{U}_l & \text{if} \quad x < x_d, \\ \mathbf{U}_r & \text{if} \quad x > x_d, \end{cases}$$

Riemann Problems

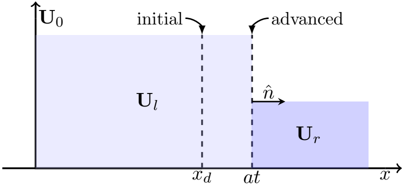

$$\frac{\partial \mathbf{U}}{\partial t} + \frac{\partial \mathbf{F}}{\partial \mathbf{x}} = \mathbf{0} \ ,$$

$$\mathbf{U}_0 = \begin{cases} \mathbf{U}_l & \text{if} \quad x < x_d, \\ \mathbf{U}_r & \text{if} \quad x > x_d, \end{cases}$$

- Solution at time t.
- Wave speed: a.

$$\mathbf{U} = \begin{cases} \mathbf{U}_l & \text{if} \quad x < at, \\ \mathbf{U}_r & \text{if} \quad x > at, \end{cases}$$

Compressible hydrodynamics

$$
\begin{aligned}
\frac{\partial \rho}{\partial t} + \nabla \cdot (\rho \mathbf{v}) = 0 \ , \\
\frac{\partial (\rho \mathbf{v})}{\partial t} + \nabla \cdot [\rho \mathbf{v} \otimes \mathbf{v} + p_g] = 0 \ , \\
\frac{\partial E}{\partial t} + \nabla \cdot [(E + p_g)\, \mathbf{v}] = 0 \ ,
\end{aligned}
$$

where the energy density is defined as

$$
E = \frac{p_g}{\gamma - 1} + \frac{\rho v^2}{2} \ ,
$$

Compressible hydrodynamics

The Euler equations are strictly hyperbolic.
1D conservative form

$$\frac{\partial \mathbf{U}}{\partial t} + \frac{\partial \mathbf{F}}{\partial x} = 0.$$

Jacobian $\mathbf{J}(\mathbf{U}) = \partial \mathbf{F}/\partial \mathbf{U}$ has three real and distinct eigenvalues:

$$\begin{aligned} \lambda_3 &= v_n + a : \text{rarefaction or shock} \\ \lambda_2 &= v_n \qquad : \text{contact discontinuity} \\ \lambda_1 &= v_n - a : \text{rarefaction or shock} \end{aligned}$$

where $a = \sqrt{\gamma p_g/\rho}$ is the speed of sound.

HLL family of approximate Riemann solvers

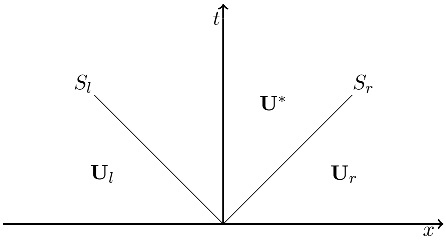

- The solver of Harden-Lax-van Leer-Einfeldt (HLLE) [2] assumes a one state solution.
- The solution approximated as weighted average of the left and right states.

HLL family of approximate Riemann solvers

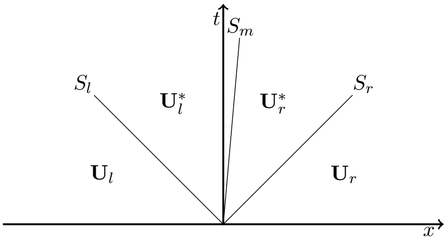

- The solver of Harden-Lax-van Leer-Einfeldt (HLLE) [2] assumes a one state solution.
- The solution approximated as weighted average of the left and right states.
- HLLC [9] (C for *contact*) restores the contact discontinuity.

HLL family of approximate Riemann solvers

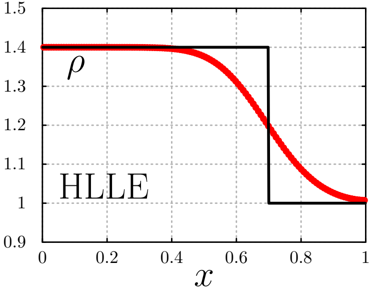

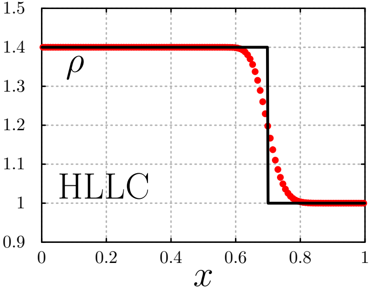

- The solver of Harden-Lax-van Leer-Einfeldt (HLLE) [2] assumes a one state solution.
- The solution approximated as weighted average of the left and right states.
- HLLC [9] (C for *contact*) restores the contact discontinuity.
- HLLC less diffuse at contact discontinuity.

Ideal magnetohydrodynamics

$$\frac{\partial \rho}{\partial t} + \nabla \cdot (\rho \mathbf{v}) = 0 \ ,$$

$$\frac{\partial (\rho \mathbf{v})}{\partial t} + \nabla \cdot \left[\rho \mathbf{v} \otimes \mathbf{v} + \left(p_g + \frac{B^2}{2} \right) \underline{\mathbf{I}} - \mathbf{B} \otimes \mathbf{B} \right] = 0 \ ,$$

$$\frac{\partial E}{\partial t} + \nabla \cdot \left[\left(E + p_g + \frac{B^2}{2} \right) \mathbf{v} - \mathbf{v} \cdot \mathbf{B} \otimes \mathbf{B} \right] = 0 \ , \text{ and}$$

$$\frac{\partial \mathbf{B}}{\partial t} + \nabla \cdot [\mathbf{v} \otimes \mathbf{B} - \mathbf{B} \otimes \mathbf{v}] = 0 \ ,$$

where the energy density is defined as

$$E = \frac{p_g}{\gamma - 1} + \frac{\rho v^2}{2} + \frac{B^2}{2} \ ,$$

Ideal magnetohydrodynamics

The ideal MHD equations are non-strictly hyperbolic. 1D conservative form

$$\frac{\partial \mathbf{U}}{\partial t} + \frac{\partial \mathbf{F}}{\partial x} = 0.$$

Jacobian $\mathbf{J}(\mathbf{U}) = \partial \mathbf{F}/\partial \mathbf{U}$ has seven real, but not necessarily distinct eigenvalues:

$$\begin{aligned} v_n &: \text{contact or tangential discontinuity (entropy)}, \\ v_n \pm c_s &: \text{slow rarefaction or shock}, \\ v_n \pm c_a &: \text{rotational discontinuity (Alfvén), and} \\ v_n \pm c_f &: \text{fast rarefaction or shock}, \end{aligned}$$

$$c_{f,s}^2 = \frac{1}{2}\left[a^2 + c_a^2 + c_t^2 \pm \sqrt{\left(a^2 + c_a^2 + c_t^2\right)^2 - 4a^2 c_a^2}\right],$$

$$c_a^2 = \frac{B_n^2}{\rho}, \text{ and } c_t^2 = \frac{B_t^2}{\rho}.$$

Ideal magnetohydrodynamics

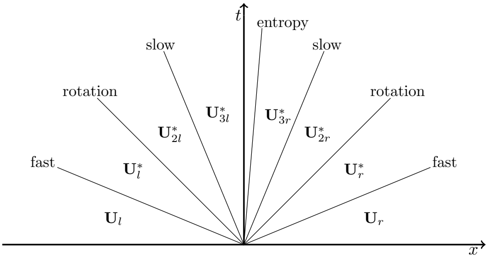

$$
\begin{aligned}
v_n &: \text{contact or tangential discontinuity (entropy)},\\
v_n \pm c_s &: \text{slow rarefaction or shock},\\
v_n \pm c_a &: \text{rotational discontinuity (Alfvén), and}\\
v_n \pm c_f &: \text{fast rarefaction or shock},
\end{aligned}
$$

Extension of HLLC for MHD

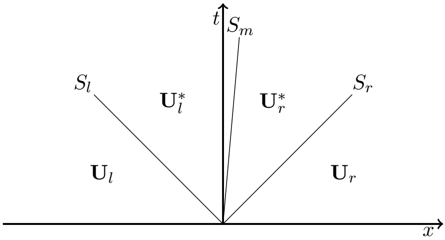

- HLLD [6] (D for *discontinuities*) extention of HLLC to MHD.

Extension of HLLC for MHD

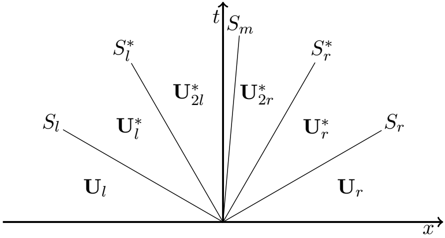

- HLLD [6] (D for *discontinuities*) extention of HLLC to MHD.
- Captures all linear discontinuities, contact and rotational.

Higher order extensions

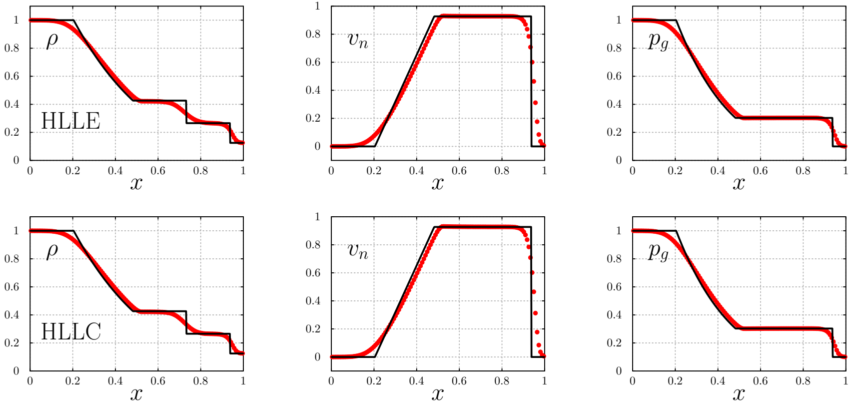

- Increase accuracy and preserve monotonicity.
- Total variation diminishing (TVD).
- Limit slope to ensure no new extrema are created.

Higher order extensions

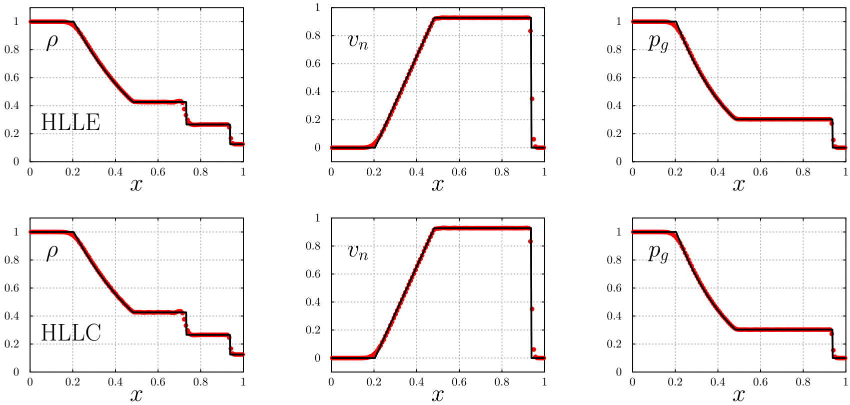

- Increase accuracy and preserve monotonicity.
- Total variation diminishing (TVD).
- Limit slope to ensure no new extrema are created.

Higher order extensions

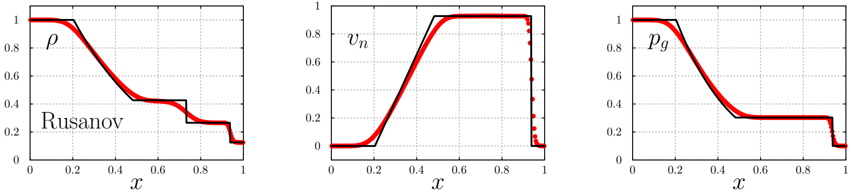

- Increase accuracy and preserve monotonicity.
- Flux corrected transport (FCT).
- Limit fluxes so that no new extrema are created.

Higher order extensions

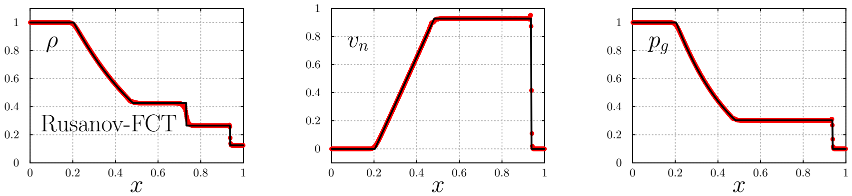

- Increase accuracy and preserve monotonicity.
- Flux corrected transport (FCT).
- Limit fluxes so that no new extrema are created.

Riemann problems of ideal MHD

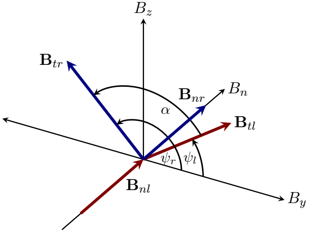

- Initial discontinuity separates two states.
- Rotation angle $\arctan B_z/B_y$.
- The initial twist angle $\alpha = \psi_r - \psi_l$.

Riemann problems of ideal MHD

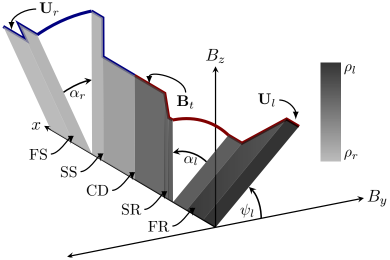

- Seven waves propagate away from initial discontinuity creating eight distinct states.

Riemann problems of ideal MHD

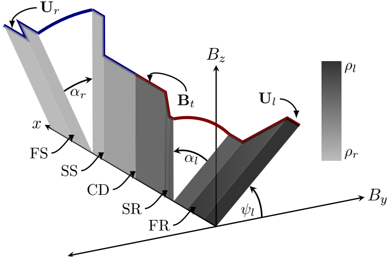

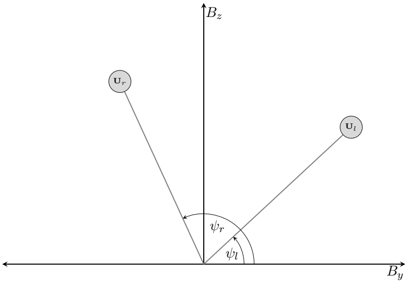

- Regular waves only alter the magnitude or orientation of B_t.

Riemann problems of ideal MHD

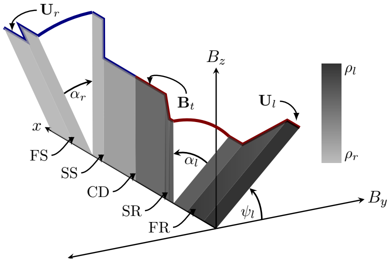

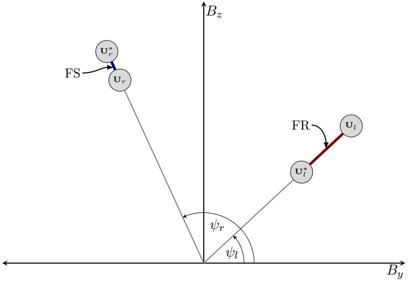

- Regular waves only alter the magnitude or orientation of B_t.
- B_t increases across fast shock, decreases across fast rarefaction.

Riemann problems of ideal MHD

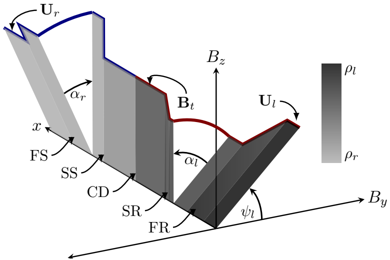

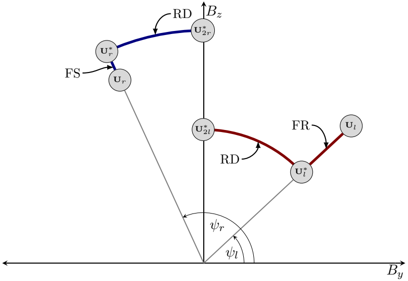

- Regular waves only alter the magnitude or orientation of B_t.
- B_t increases across fast shock, decreases across fast rarefaction.
- B_t changes orientation across a rotational discontinuity.

Riemann problems of ideal MHD

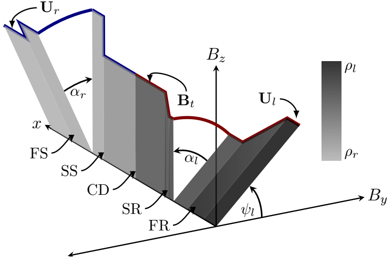

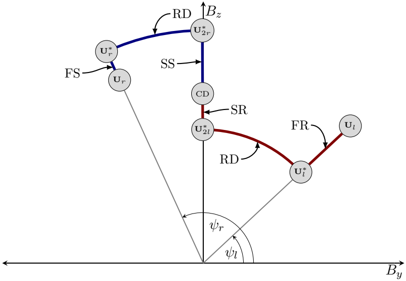

- Regular waves only alter the magnitude or orientation of B_t.
- B_t increases across fast shock, decreases across fast rarefaction.
- B_t changes orientation across a rotational discontinuity.
- B_t decreases across slow shock, increases across slow rarefaction.

Riemann problems of ideal MHD

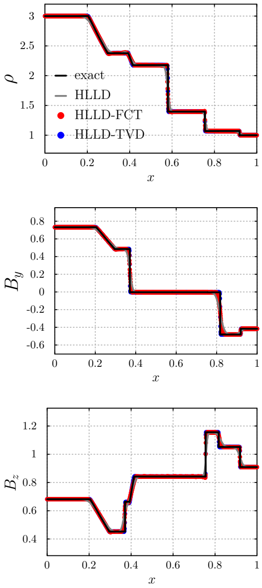

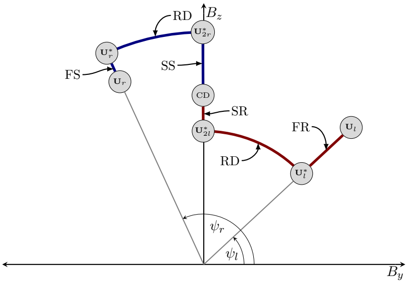

Non-unique solutions

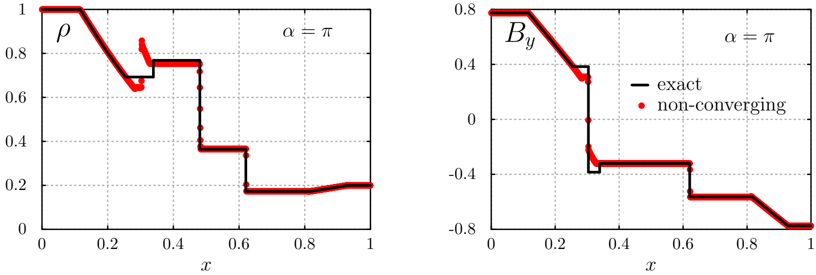

- Solutions to coplanar Riemann problems of ideal MHD are non-unique.
- At $x = 0.303$, rotational discontinuity $\rightarrow$ compound wave.

Non-unique solutions

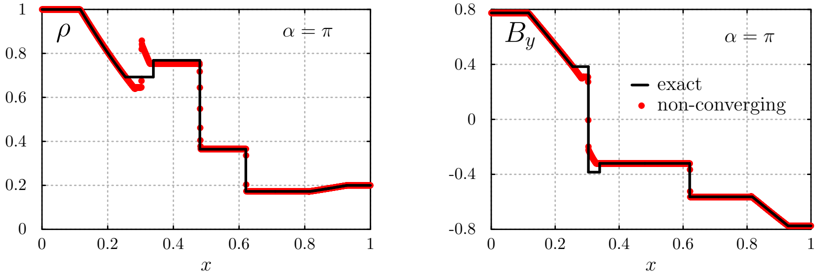

- Solutions to coplanar Riemann problems of ideal MHD are non-unique.
- At $x = 0.303$, rotational discontinuity $\rightarrow$ compound wave.
- Compound wave is composed of an intermediate shock and a slow rarefaction.
- Physical?
- Unstable for under small perturbations [5].
- Satisfies jump conditions in the coplanar case.

Non-unique solutions

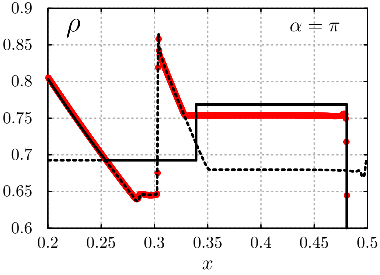

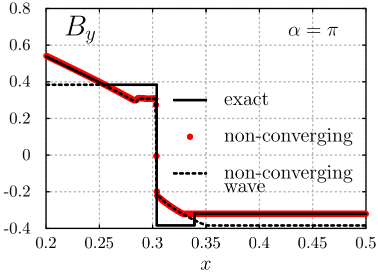

- An intermediate shock is a non-regular, i.e., not a Lax shock, wave that changes the orientation of the magnetic field.
- Slow compound wave: super-Alfvénic $\rightarrow$ sub-slow.
- In shock frame upstream: $c_a < v_n < c_f$

$$v_n = 1.0174, c_a = 0.9661, c_f = 1.1295$$

- In shock frame downstream: $v_n < c_s, c_a$

$$v_n = 0.7341, c_s = 0.8033, c_a = 0.8222$$

Psuedo-convergence

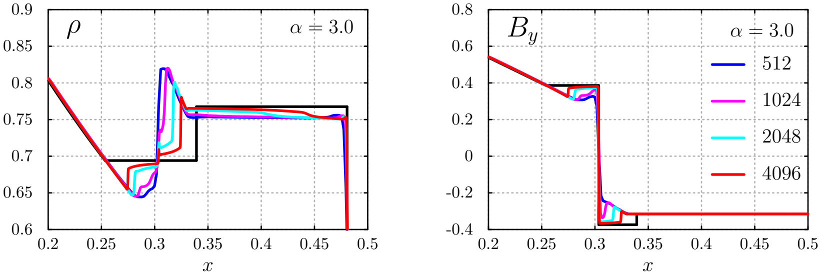

- Near-coplanar case, compound waves present at lower resolutions.
- Psuedo-convergence: increasing resolution produces convergence to regular wave solution [10].
- The compound waves begin to break apart between 1024 and 2048 grid points.
- As $\alpha \to \pi$, grid resolution increases.
- When $\pi = \alpha$, compound wave at all resolutions.

Compound Wave modification

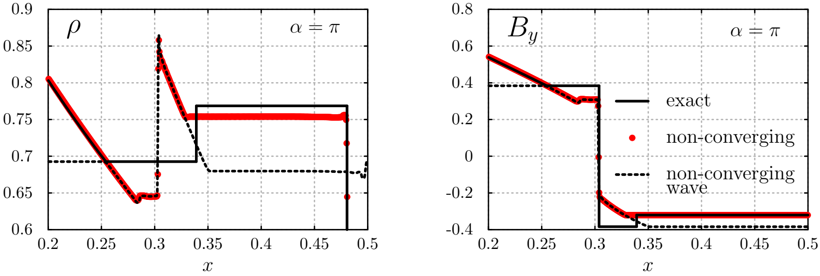

- Compound waves are product of numerical diffusion for near coplanar problems.
- Reduce diffusion to recover correct solution. How?

Compound Wave modification

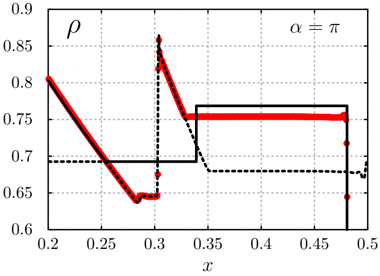

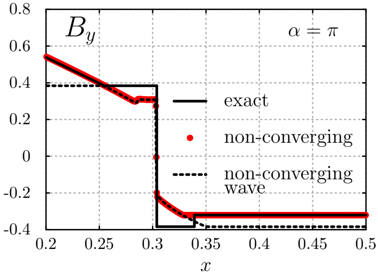

- Compound waves are product of numerical diffusion for near coplanar problems.
- Reduce diffusion to recover correct solution. How?
- ρ and B_t should remain constant across the rotational discontinuity $x = 0.303$.

Compound Wave modification

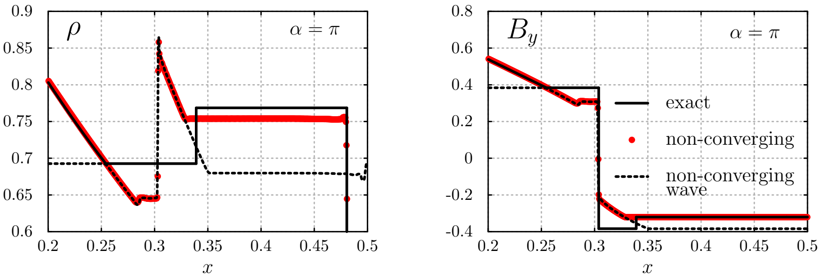

- Compound waves are product of numerical diffusion for near coplanar problems.
- Reduce diffusion to recover correct solution. How?
- ρ and B_t should remain constant across the rotational discontinuity $x = 0.303$.
- Limit flux associated with the compound wave.

Compound Wave modification

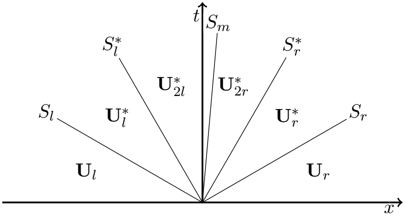

- Use HLLD to approximate intermediate states upstream and downstream of rotational discontinuity, i.e., $\mathbf{U}_l^*$ and $\mathbf{U}_{2l}^*$.

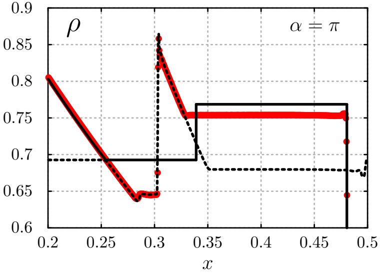

Compound Wave modification

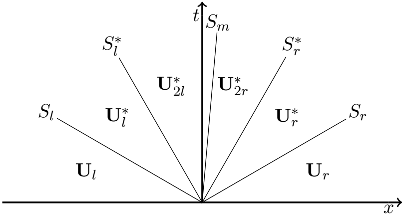

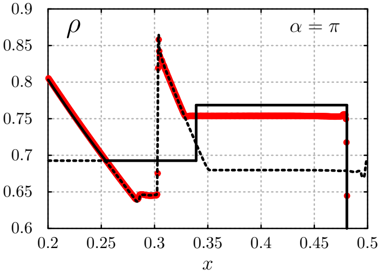

- Use HLLD to approximate intermediate states upstream and downstream of rotational discontinuity, i.e., $\mathbf{U}_l^*$ and $\mathbf{U}_{2l}^*$.
- Calculate flux $\mathbf{F}^c$ between $\mathbf{U}_l^*$ and $\mathbf{U}_{2l}^*$ responsible for formation of the compound wave.

Compound Wave modification

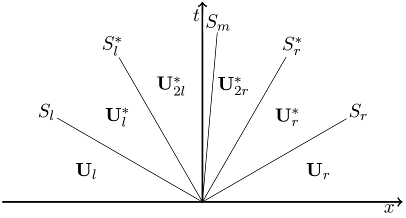

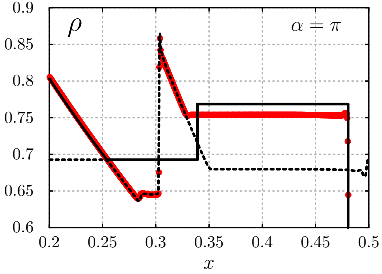

- Use HLLD to approximate intermediate states upstream and downstream of rotational discontinuity, i.e., $\mathbf{U}_\mathbf{l}^*$ and $\mathbf{U}_{2l}^*$.
- Calculate flux $\mathbf{F}^c$ between $\mathbf{U}_\mathbf{l}^*$ and $\mathbf{U}_{2l}^*$ responsible for formation of the compound wave.
- Reduce the contribution of $\mathbf{F}^c = \mathbf{F}_{hlld}(\mathbf{U}_l^*, \mathbf{U}_{l2}^*)$ to the total flux.

Compound Wave modification

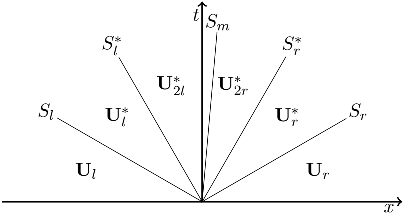

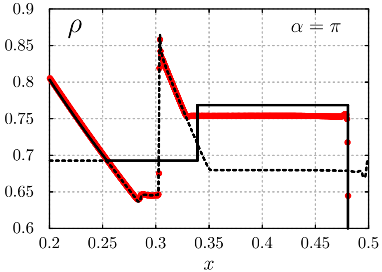

- Use HLLD to approximate intermediate states upstream and downstream of rotational discontinuity, i.e., $\mathbf{U}_l^*$ and $\mathbf{U}_{2l}^*$.
- Calculate flux $\mathbf{F}^c$ between $\mathbf{U}_l^*$ and $\mathbf{U}_{2l}^*$ responsible for formation of the compound wave.
- Reduce the contribution of $\mathbf{F}^c = \mathbf{F}_{hlld}(\mathbf{U}_l^*, \mathbf{U}_{l2}^*)$ to the total flux.
- $\mathbf{F}_{cwm} = \mathbf{F}_{hlld}(\mathbf{U}_l, \mathbf{U}_r) - A\mathbf{F}^c$, where $A < 0.5$.

CWM Results

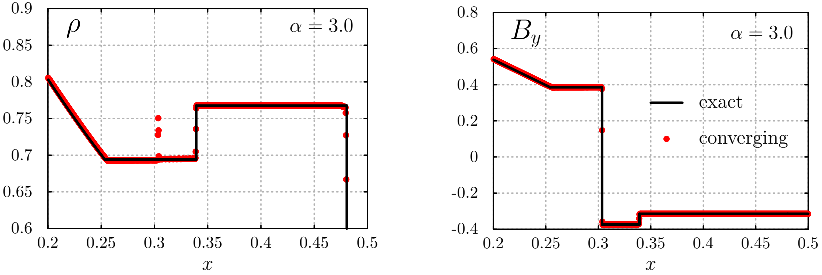

- CWM recovers the correct solution upstream and downstream of rotational discontinuity.
- Transition across rotational discontinuity is unresolved.
- Resolve it?

CWM Results

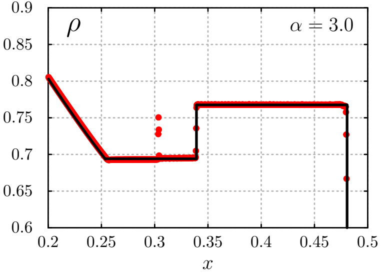

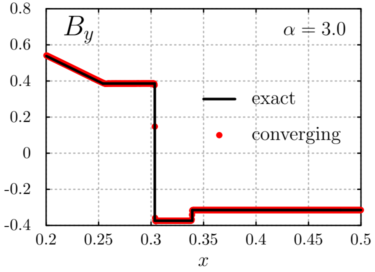

- CWM recovers the correct solution upstream and downstream of rotational discontinuity.
- Transition across rotational discontinuity is unresolved.
- Resolve it?
- Simple but non-conservative.

CWM Resolving the transition

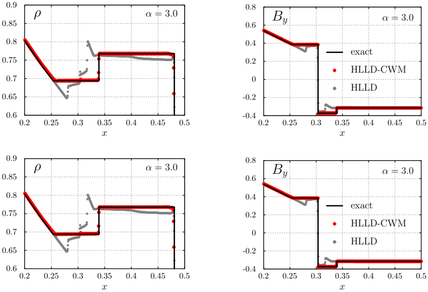

- Jump conditions in Lagrangian mass coordinates, $V = 1/\rho$, W is wave speed.
- Brackets denote difference across discontinuity.

$$
\begin{aligned}
W[V] &= -[v_n], \\
W[v_n] &= -[P - B_n^2], \\
W[\mathbf{v}_t] &= -B_n[\mathbf{B}_t], \\
W[V\mathbf{B}_t] &= -B_n[\mathbf{v}_t],
\end{aligned}
$$

CWM Resolving the transition

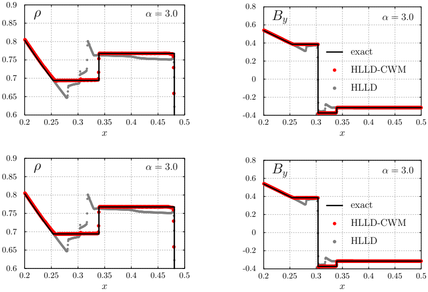

- Across rotational discontinuity

$$
\begin{aligned}
[V] &= 0, \\
[v_n] &= 0, \\
[p_g] &= 0, \\
[B_t] &= 0, \\
W[\mathbf{v}_t] &= -B_n[\mathbf{B}_t],
\end{aligned}
$$

- $W = \sqrt{\rho} B_n$ is Lagrangian speed of linear wave.

Results

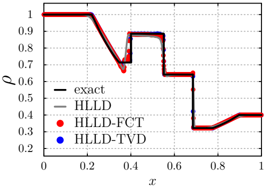

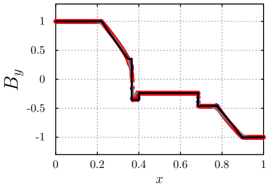

- Near coplanar initial conditions.
- Fast compound wave at $x = 0.365$

Results

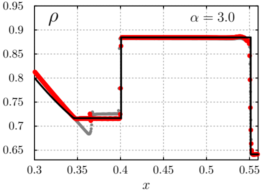

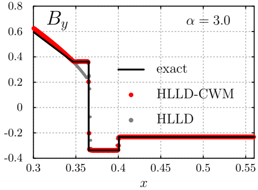

- Near coplanar initial conditions.
- Fast compound wave at $x = 0.365$
- Small deviation for weak intermediate shocks.

Results

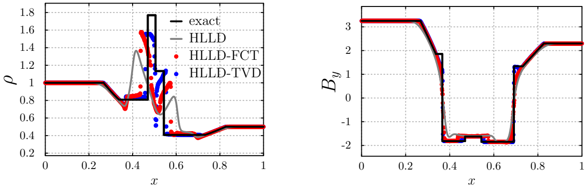

- Non-planar initial conditions.
- Fast compound waves at $x = 0.366$ and $x = 0.691$

Results

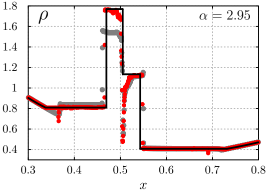

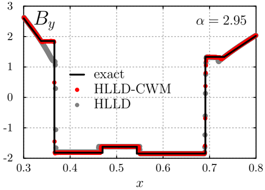

- Non-planar initial conditions.
- Fast compound waves at $x = 0.366$ and $x = 0.691$
- Small deviation for weak intermediate shocks.

Error analysis

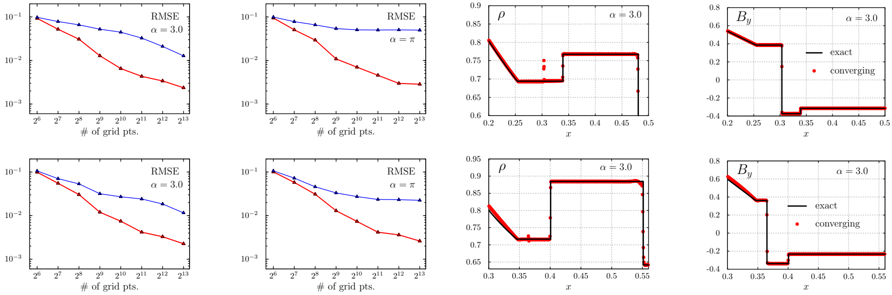

- Error calculation without applying the correction at the rotational discontinuity.
- Without CWM, the compoiund wave starts to break apart between 2^{10} and 2^{11}.
- CWM produces convergence at low grid resolutions.

Higher dimensions

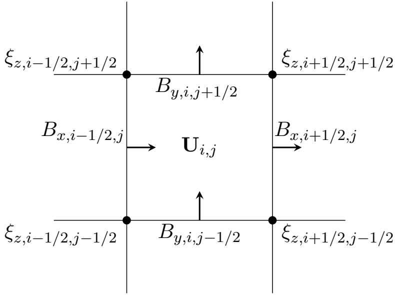

Maintaining $\nabla \cdot \mathbf{B} = 0$ with constrained transport [3].

- Staggered grid.
- Hydrodynamical variables at cell centers.
- Magnetic field at interface.
- $\mathbf{E} = -\mathbf{v} \times \mathbf{B}$ at corners.
- Denote z-component of the emf as ξ_z.

Finite area integration of interface **B**

$$B^{n+1}_{x,i+1/2,j} = B^{n}_{x,i+1/2,j} - \frac{\delta t}{\delta y} \left(\xi_{z,i+1/2,j+1/2} - \xi_{z,i+1/2,j-1/2}\right)$$
$$B^{n+1}_{y,i,j+1/2} = B^{n}_{y,i,j+1/2} + \frac{\delta t}{\delta x} \left(\xi_{z,i+1/2,j+1/2} - \xi_{z,i-1/2,j-1/2}\right)$$

Higher dimensions

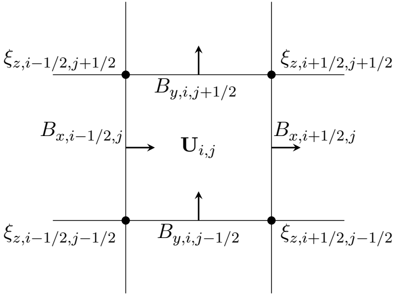

Maintaining $\nabla \cdot \mathbf{B} = 0$ with constrained transport [3].

- Staggered grid.
- Hydrodynamical variables at cell centers.
- Magnetic field at interface.
- $\mathbf{E} = -\mathbf{v} \times \mathbf{B}$ at corners.
- Denote z-component of the emf as ξ_z.

Due to perfect cancellation, the numerical divergence in the cell remains zero to machine precision.

$$(\nabla \cdot \mathbf{B})_{i,j} = \frac{1}{\delta x}\left(B_{x,i+1/2,j} - B_{x,i-1/2,j}\right) + \frac{1}{\delta y}\left(B_{y,i,j+1/2} - B_{y,i,j-1/2}\right)$$

Shared memory parallelism

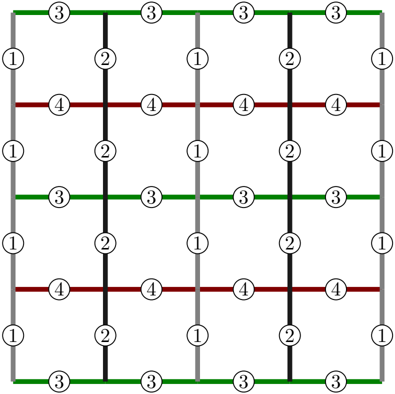

- Faces must be grouped by color to avoid memory contention.
- Loop over the faces becomes loop over the colors.

Shared memory parallelism

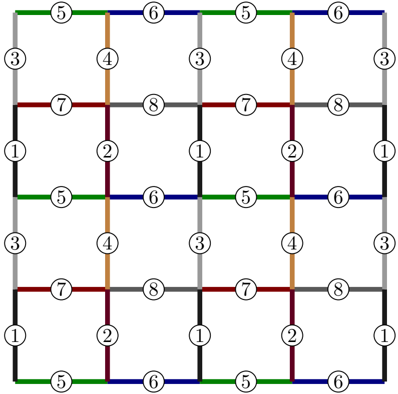

- Faces must be grouped by color to avoid memory contention.
- Loop over the faces becomes loop over the colors.
- Constrained transport, faces and edges must be colored.

Efficient algorithms

```
thrust::device_vector<float> x(n);  // independent
    variable
thrust::device_vector<float> y(n);  // y = f(x)
thrust::device_vector<float> z(n);  // z = g(y)

// compute y = f(x)
thrust::transform(x.begin(),x.end(),y.begin(),f());

// compute z = g(y)
thrust::transform(y.begin(),y.end(),z.begin(),g());
```

- Function composition [4].
- $3n$ floats, $2n$ reads, $2n$ writes, and uses n temporary floats.

Efficient algorithms

```
thrust::device_vector<float> x(n);  // independent
    variable
thrust::device_vector<float> z(n);  // z = g(y) = g(
    f(x))

// compute z = g(f(x))
thrust::transform(make_transform_iterator(x.begin(),
    f()),
                  make_transform_iterator(x.end(),f
                      ()),
                  z.begin(),
                  g());
```

- Function composition [4].
- $2n$ floats, n reads, n writes, and no temporary storage.

Efficient algorithms

```
thrust::device_vector<float> x(n);  // independent
    variable
thrust::device_vector<float> z(n);  // z = g(y) = g(
    f(x))

// compute z = g(f(x))
thrust::transform(make_transform_iterator(x.begin(),
    f()),
                  make_transform_iterator(x.end(),f
                      ()),
                  z.begin(),
                  g());
```

- Function composition [4].
- $2n$ floats, n reads, n writes, and no temporary storage.

Memory access

```
struc
    conservative_variables{
  float density;
  float momentum_x;
  float energy;
}

conservative_variables
  *state;  // AoS

state[i].density =
    some_number;
state[i].momentum_x =
    another_number;
state[i].energy =
    one_more_number;
```

```
struc
    conservative_variables{
  float *density;
  float *momentum_x;
  float *energy;
}

conservative_variables
    state; // SoA

state.density[i] =
    some_number;
state.momentum_x[i] =
    another_number;
state.energy[i] =
    one_more_number;
```

- Memory coalescing occurs when multiple memory addresses are accessed with a single transaction.
- Memory does not coalesce with AoS (left).
- Memory does coalesce with SoA (right).

Memory access

```
thrust::device_vector<primitive_variables>
     primitive_state(n);  // AoS
thrust::device_vector<conservative_variables>
     conservative_state(n);   // AoS
thrust::transform_n(primitive_state.begin(),
                    primitive_state.size(),
                    conservative_state.begin(),
                    convert_primitive_to_conservative(
                        gamma));
```

- Converting from primitive variables (ρ, v_x, p_g) to conservative variables $(\rho, \rho v_x, en)$.
- No coalescing.

Memory access

```
thrust::device_vector<float> d(n),vx(n),pg(n);
thrust::device_vector<float> mx(n),en(n);
thrust::transform_n(
          thrust::make_zip_operator(
            make_tuple(d.begin(),
                       vx.begin(),
                       pg.begin())),
           n,
           thrust::make_zip_operator(
             make_tuple(d.begin(),
                        mx.begin(),
                        en.begin())),
           convert_primitive_to_conservative(gamma));
```

- Converting from primitive variables (ρ, v_x, p_g) to conservative variables $(\rho, \rho v_x, en)$.
- Arrays can be combined on the fly with a `zip_operator` to achieve coalescing.

Performance Comparison

Table: Performance comparison for Orszag-Tang [7] test.

grid size	cells/second (GPU)	cells/second (CPU)	ratio
64×64	4.1894×10^6	7.3955×10^5	5
128×128	1.6540×10^7	7.5060×10^5	22
256×256	4.4497×10^7	7.3155×10^5	60
512×512	6.3286×10^7	7.9437×10^5	79
1024×1024	7.2134×10^7	8.3354×10^5	86

- Dell Precision 7500 workstation with a (Dual CPU)
- CPU Intel Xeon E5645 @ 2.40 Ghz.
- GPU GeFroce GTX TITAN with a memory bandwidth of 288.4 GB/sec and 2688 CUDA cores.
- Almost a factor of three increase of speed ratio form 128×128 to 256×256.

Conclusion

- Provided new benchmarks for MHD model development.
- Released* a nonlinear solver for ideal MHD.
- Developed the compound wave modification:
  - First method able to produce the rotational discontinuity for coplanar Riemann problems of ideal MHD without using a nonlinear solver.
  - First method to avoid pseudo-convergence for near coplanar problems of ideal MHD.
  - FAST! HLLD intermediate states are already calculated, modification for little cost.
  - Produces the correct result when other numerical inaccuracies are present.
- Released* a high-order multi-dimensional fluid solver.
  - Algorithms implemented for general geometry on unstructured grids.
  - Capable of shared memory parallelism on GPU and CPU.
  - Can be used as blueprint or benchmark by anyone in computational physics and space weather communities wishing to increase performance.

Bibliography I

[1] H. de Sterck, B. C. Low, and S. Poedts. “Complex magnetohydrodynamic bow shock topology in field-aligned low-β flow around a perfectly conducting cylinder”. In: *Physics of Plasmas* 5 (Nov. 1998), pp. 4015–4027.

[2] B. Einfeldt. “On Godunov-Type Methods for Gas Dynamics”. In: *SIAM J. Numer. Anal.* 25 (1988), pp. 294–318.

[3] C. R. Evans and J. F. Hawley. “Simulation of magnetohydrodynamic flows - A constrained transport method”. In: *ApJ* 332 (Sept. 1988), pp. 659–677.

[4] Jared Hoberock and Nathan Bell. *Thrust: A Parallel Template Library*. Version 1.7.0. 2010. URL: `http://thrust.github.io/`.

[5] L. D. Landau, E. M. Lifshitz, and L. P. Pitaevskii. *Electrodynamics of continuous media*. 3rd. 1984.

Bibliography II

[6] T. Miyoshi and K. Kusano. “A multi-state HLL approximate Riemann solver for ideal MHD”. In: *J. Comp. Phys.* 208 (May 2005), pp. 315–344.

[7] S. A. Orszag and C.-M. Tang. “Small-scale structure of two-dimensional magnetohydrodynamic turbulence”. In: *Journal of Fluid Mechanics* 90 (Jan. 1979), pp. 129–143.

[8] G. A. Sod. “A survey of several finite difference methods for systems of nonlinear hyperbolic conservation laws”. In: *J. Comp. Phys.* 27 (Apr. 1978), pp. 1–31.

[9] E. F. Toro, M. Spruce, and W. Speares. “Restoration of the contact surface in the HLL-Riemann solver”. In: *Shock Waves* 4 (Mar. 1994), pp. 25–34.

Bibliography III

[10] M. Torrilhon. "Non-uniform convergence of finite volume schemes for Riemann problems of ideal magnetohydrodynamics". In: *J. Comp. Phys.* 192 (Nov. 2003), pp. 73–94.